J Mater Sci (2007) 42:9888–9893
DOI 10.1007/s10853-007-1630-x

Fatigue crack propagation behavior of friction stir welded 5083-H32 Al alloy

Seongjin Hong · Sangshik Kim · Chang Gil Lee · Sung-Joon Kim

Received: 7 August 2006 / Accepted: 20 February 2007 / Published online: 18 August 2007

Abstract Fatigue crack propagation (FCP) behavior of friction stir welded (FSWed) 5083-H32 Al alloy was examined with the fatigue crack growing either along the dynamically recrystallized zone (DXZ) at variable ΔK or perpendicular to the DXZ at a constant ΔK value of 10, 13, 15, and 17 MPa$\sqrt{\text{m}}$, respectively. The FCP behavior of FSWed 5083-H32 specimen is substantially influenced by the presence of FSW zone, the trend of which is discussed based on residual stress measurement and fractographic observation.

Introduction

Friction stir welding (FSW) is a new solid-state joining method offering several advantages over conventional welding methods, including better mechanical properties, low residual stress and reduced occurrence of defects [1–4]. 5083 Al alloy is a non-heat treatable Al-Mg-Mn alloy developed for applications requiring a weldable moderate strength alloy having good corrosion resistance [5, 6]. As such it is an excellent all round alloy ideal for many applications including transportation and construction [7, 8]. Previously, it has been demonstrated that the tensile property reduction with FSW is not significant for 5083-H32 specimen. The tensile strength and tensile elongation of FSWed 5083-H32 are, for example, 301 MPa and 17% compared to 306 MPa and 22% for the base metal (BM) [9]. The resistance to corrosion for the FSWed 5083-H32 specimen in NaCl aqueous solution is greater than that for the BM specimen due to grain refinement in the FSW zone [10]. It has been proposed that the fatigue crack propagation (FCP) behavior of FSWed Al alloys is strongly influenced by grain refinement in the dynamically recrystallized zone (DXZ) and/or the residual stress developed in the FSW zone [11, 12]. A controversy exists for the FCP behavior of FSWed Al alloys. Pao et al. proposed that compressive residual stresses could lower the crack-tip driving force (ΔK) in the DXZ resulting in lower FCP rates and higher apparent ΔK_{th} in FSWed Al 2519 alloy [11]. Jata et al. on the other hand, suggested that fine recrystallized grains formed in the weld zone dominate the FCP behavior of FSWed Al 7050-T7451 alloy and reduce the resistance to FCP [12]. Previously the authors proposed that the FCP rates of 6061-T651 Al alloy in the DXZ tended to be significantly lower than those in the BM particularly in low ΔK regime [13]. The FCP behavior of FSWed 6061-T651 in the DXZ appeared to be determined by the beneficial compressive residual stress reducing effective ΔK and the detrimental grain refinement causing intergranular fatigue failure. At present, very little research has been conducted on FCP behavior of FSWed Al-Mg-Mn alloy, which impedes the wider use of this versatile weldable Al alloy [14].

The objective of this study is to examine the FCP behavior of FSWed 5083-H32 Al alloy. The FCP rates for FSWed Al 5083-H32 specimen were measured with the fatigue crack growing either along the DXZ at variable ΔK or perpendicular to the DXZ at a constant ΔK value of 10, 13, 15, and 17 MPa$\sqrt{\text{m}}$, respectively. The FCP behavior of

S. Hong · S. Kim (✉)
Division of Materials Science and Engineering, Engineering Research Institute, Gyeongsang National University, Chinju, Korea
e-mail: sang@gsnu.ac.kr

C. G. Lee · S.-J. Kim
Institute of Materials Science and Technology, Korea Institute of Machinery and Materials, Changwon, Korea

FSWed 5083-H32 Al alloy was discussed based on the micrographic and fractographic observation and residual stress measurement.

Experimental procedure

The 4 mm thick 5083-H32 Al alloy plates were FSWed at a tool rotating speed of 1,600 rpm and a welding speed of 0.25 mpm (m/min). Previous studies on the effect of various FSW condition on tensile behavior of 5083-H32 Al alloy showed that the present rotating and welding speed combination rendered the best tensile property for this alloy [9]. Table 1 represents the tensile properties of base metal (BM) and FSWed 5083-H32 specimens. Cross-sectional macrographic view was documented with the specimen etched with modified Poulton's reagent (40 mL HNO_3 + 12 g H_2CrO_4 + 30 mL HCl + 2.5 mL HF + 42.5 mL H_2O). For quantitative grain size measurement, electron backscatter diffraction (EBSD) technique was used. Compact tension (CT) specimens with a width (W) of 50.8 mm and a thickness (B) of 4.0 mm were prepared from the FSWed plate. FCP experiments were conducted at an R ratio of 0.1 and a sinusoidal frequency of 10 Hz with the fatigue crack growth either along the DXZ with variable ΔK or perpendicular to the DXZ at constant ΔK of 10, 13, 15, and 17 MPa$\sqrt{\text{m}}$, respectively, on an Instron model 8516 servo-hydraulic testing machine. Figure 1 shows the schematic illustration of CT specimens used for (a) variable ΔK and (b) constant ΔK FCP test, respectively. The macrographic cross-sectional views for the FSWed 5083-H32 specimen are also included. The FCP rates were measured by using a DCPD (direct current potential drop) technique. Residual stress analyses were performed on top surface of the FSWed plate either perpendicular ($\sigma_{res,t}$) or parallel ($\sigma_{res,l}$) to the weld zone axis using Rigaku model D/MAX-3C X-ray diffractometer. The residual stresses distribution is obtained using $\sin^2\psi$ method [15]. The fractographs for the fatigue fractured specimens were examined by using scanning electron microscope (SEM).

Results and discussion

Previously, it was proposed that the FCP behavior of FSWed, heat-treatable Al alloys, including 2519 [11], 7050

Table 1 Tensile properties of BM and FSWed 5083-H32 specimens

Condition	Yield strength (MPa)	Ultimate tensile strength (MPa)	Tensile elongation (%)
BM	137	306	22.0
FSWed	150	301	17.0

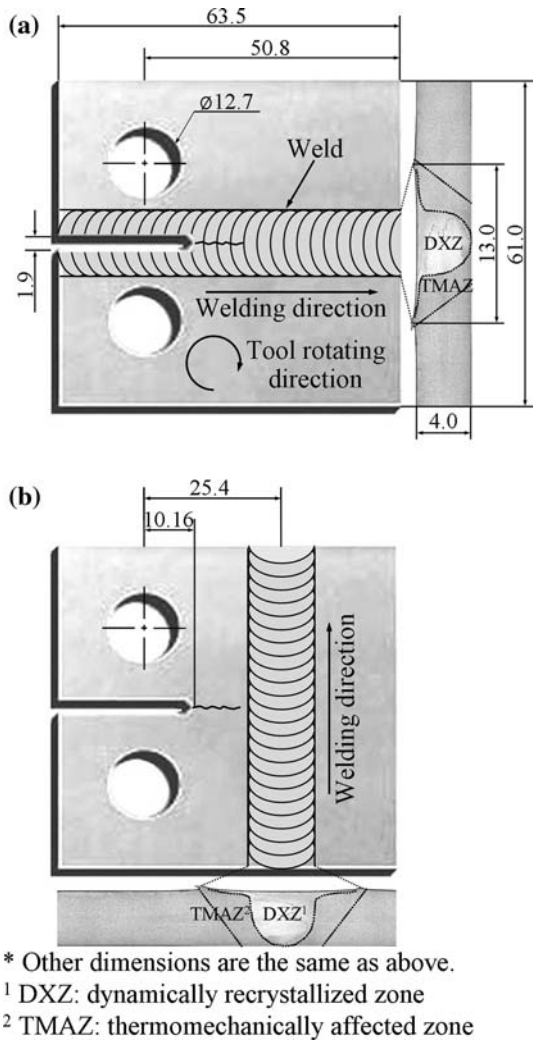

Fig. 1 Schematic illustration of CT specimens used for (**a**) variable ΔK and (**b**) constant ΔK FCP test, respectively (unit: mm)

[12], and 6061 [13], is strongly influenced by grain refinement and residual stress developed in the FSW zone. Figure 2 shows (a) the macroscopic optical micrograph and the EBSD images for the FSWed 5083-H32 specimen in the (b) dynamically recrystallized zone (DXZ), (c) thermomechanically affected zone (TMAZ), and (d) base metal (BM), respectively, cross-sectioned perpendicular to the welding direction. Table 2 summarizes the grain size measurement for each zone obtained from Fig. 2(b)–(d) showing that the DXZ has much finer grain structure compared to the BM due to dynamic recrystallization during FSW process. A number of studies have reported that compressive residual stress develops both longitudinal and transverse to the weld in the FSWed specimen due to complex thermal and rigid clamping used during FSW process [16, 17]. Figure 3 shows (a) transverse ($\sigma_{res,t}$) and (b) longitudinal ($\sigma_{res,l}$) residual stress distribution for the

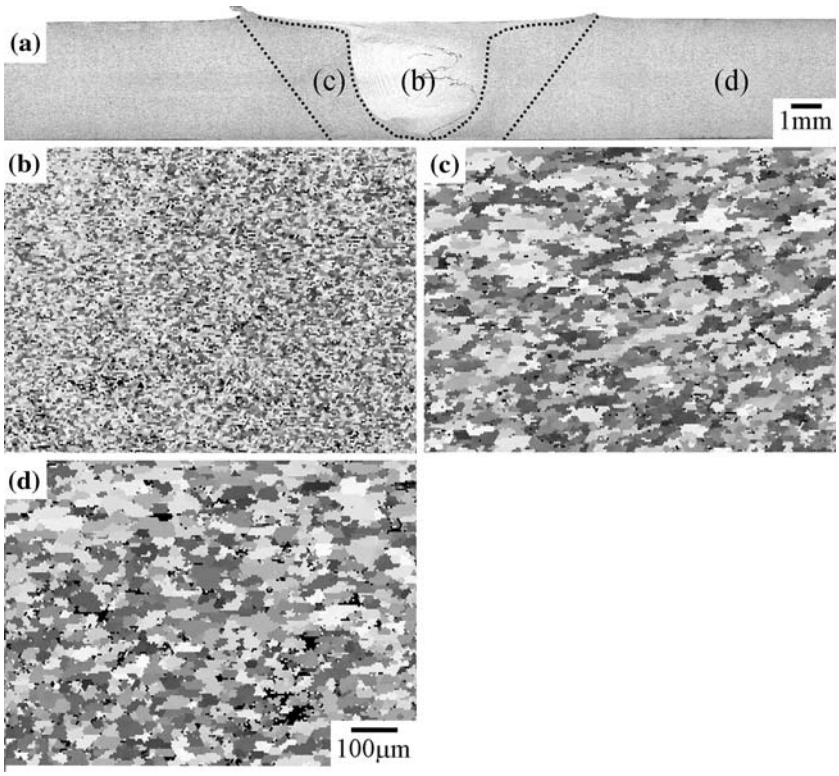

Fig. 2 Typical (**a**) macroscopic optical micrograph and the EBSD images for the FSWed 5083-H32 specimen in the (**b**) dynamically recrystallized zone (DXZ), (**c**) thermomechanically affected zone (TMAZ), and (**d**) base metal (BM), respectively, cross-sectioned perpendicular to the welding direction

Table 2 Average grain sizes for the BM, TMAZ, and DXZ, respectively, for the FSWed 5083-H32 specimen

Location	BM	TMAZ	DXZ
Average grain size (μm)	19.0	16.1	8.2

FSWed 5083-H32 specimen as a function of distance from the weld zone axis. Figure 3(c) represents the locations and the directions of residual stress measurement. Figure 3(a) indicates that average compressive residual stress of approximately −19 MPa exists across the weld zone ranging approximately ±10 mm from the weld zone axis perpendicular to the welding direction. Figure 3(b) shows typical "M"-like distribution of longitudinal residual stress across the weld with the maximum compressive residual stress of approximately −30 MPa on the advancing side of the weld, which is approximately 12 mm away from the weld zone axis. The optical micrographic observation

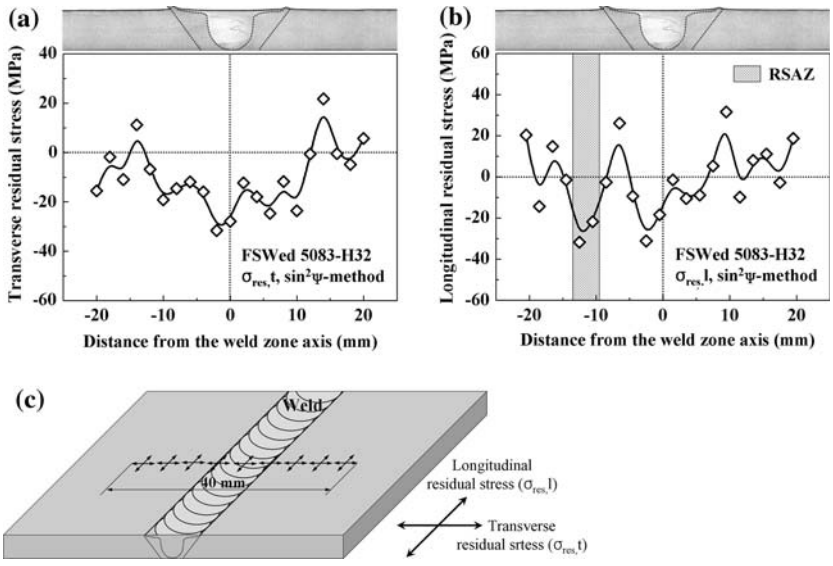

Fig. 3 Residual stress distribution for the FSWed 5083-H32 specimen either along (**a**) transverse ($\sigma_{res,t}$) or (**b**) longitudinal ($\sigma_{res,l}$) direction as a function of distance from the weld zone axis. (**c**) represents the locations and the directions for residual stress measurement

suggests that this region with maximum residual stress shows no microstructural difference compared to the BM and is designated as RSAZ (residual stress affected zone) in this study. Previously it has been suggest that such an "M"-like distribution of longitudinal residual stress is due to local frictional heating at the tool-material interface causing constraint on the BM adjacent to the TMAZ and the weld seam [18]. Unlike the advancing side, negligible tensile or compressive residual stress was noted on the retreating side. Such a mild asymmetry in longitudinal residual stress profile is often reported across the weld with the stress being higher on the advancing side [19, 20]. The asymmetry in the residual stress distribution is due to the materials flow in the weld zone is non-symmetrically distributed about the weld zone axis [19, 20].

In order to understand the effects of refined microstructure in the DXZ and residual stress on the FCP behavior of FSWed 5083-H32 specimens, two different types of fatigue crack growth tests were conducted. First, the FCP rates for FSWed 5083-H32 specimens were measured with the fatigue crack growing along the BM and the DXZ, respectively, at variable ΔK values. The second type of fatigue test consists of fatigue crack growing perpendicular to the welding direction at a constant ΔK value of 10, 13, 15, and 17 MPa$\sqrt{\text{m}}$, respectively. Figure 4 shows the da/dN–ΔK curves for the FSWed 5083-H32 specimens along the BM and the DXZ, respectively. The FCP rates for the DXZ were substantially lower than those for the BM over the entire stress intensity factor range studied. The FCP rate retardation is particularly significant in low and intermediate ΔK regimes. The near-threshold ΔK value, ΔK_{th}, was, for example, approximately 7.5 MPa$\sqrt{\text{m}}$ for the FSWed specimen compared to 4 MPa$\sqrt{\text{m}}$ for the BM specimen. As represented in Fig. 3(a), the average compressive residual stress of approximately −19 MPa exists in the DXZ of FSWed 5083-H32 specimens perpendicular to the crack propagation direction and this would decrease the FCP rates by reducing the effective ΔK. In order to quantify the compressive residual stress contribution to the FCP rates, the average residual stress of −19 ± 5 MPa was considered for calculating the da/dN–ΔK relationship of the BM specimen. The band in Fig. 4 represents the residual stress corrected da/dN–ΔK for the BM specimen, showing that the corrected FCP rates with residual stress do not match to those for the DXZ specimen. This suggests that residual stress alone cannot explain the reduced FCP rates in the DXZ. Previously, Jata et al. proposed that fine recrystallized grains formed in the DXZ could increase the FCP rates of the FSWed 7075-T7451 specimen by reducing crack closure contribution [12]. The authors also proposed that the FCP behavior of FSWed 6061-T651 in the DXZ is determined by the beneficial compressive residual stress reducing effective ΔK and the detrimental grain refinement causing intergranular fatigue failure [13]. As shown in Table 2, the average grain size of the DXZ for the FSWed 5083-H32 specimen is approximately 40% smaller than that for the BM specimen. Figure 5 shows the SEM fractographs of 5083-H32 specimens fatigued along the BM at (a) $\Delta K \approx 4$ MPa$\sqrt{\text{m}}$ and (b) $\Delta K \approx 20$ MPa$\sqrt{\text{m}}$, respectively, and the DXZ at (c) $\Delta K \approx 7.5$ MPa$\sqrt{\text{m}}$ and (d) $\Delta K \approx 20$ MPa$\sqrt{\text{m}}$, respectively. Unlike the typical cleavage facet for the BM specimen (Fig. 5(a)), intergranular FCP mode was noted for the DXZ specimen in the near-threshold ΔK regime (Fig. 5(c)). Such an intergranular fatigue crack path caused by grain refinement in the near-threshold ΔK regime would further reduce the resistance to FCP along with the reduced crack closure contribution, as proposed by Jata et al. [12]. In high ΔK regime, both specimens showed crystallographic facet fracture mode showing no notable difference. The present observation strongly suggests that the reduced FCP rates in the DXZ for the FSWed 5083-H32 specimen appears to be due to the combination of beneficial compressive residual stress effect and detrimental fine grain recrystallization.

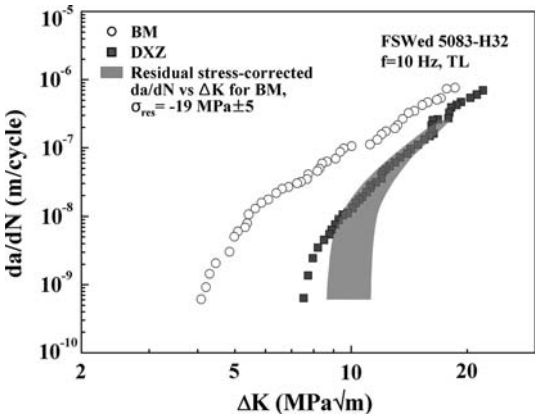

Fig. 4 da/dN–ΔK curves for the FSWed 5083-H32 specimens along the BM and the DXZ, respectively. The band in Fig. 4 represents the residual stress corrected da/dN–ΔK for the BM specimen

Practically, fatigue crack may initiate in the middle portion of structural panel and propagate across the weld zone. In this study, the FCP rates for FSWed 5083-H32 specimen were measured across the weld zone at constant ΔK value of 10, 13, 15, and 17 MPa$\sqrt{\text{m}}$, respectively. Figure 6 shows the fatigue crack length, a, as a function of fatigue loading cycle, N at each applied ΔK. The macrographic cross-sectional view and longitudinal residual stress distribution for the FSWed 5083-H32 specimen are also included on the left side of the graph to identify the location where the abrupt change in the FCP rates occurs. The change in the FCP rates, as represented by the slope of

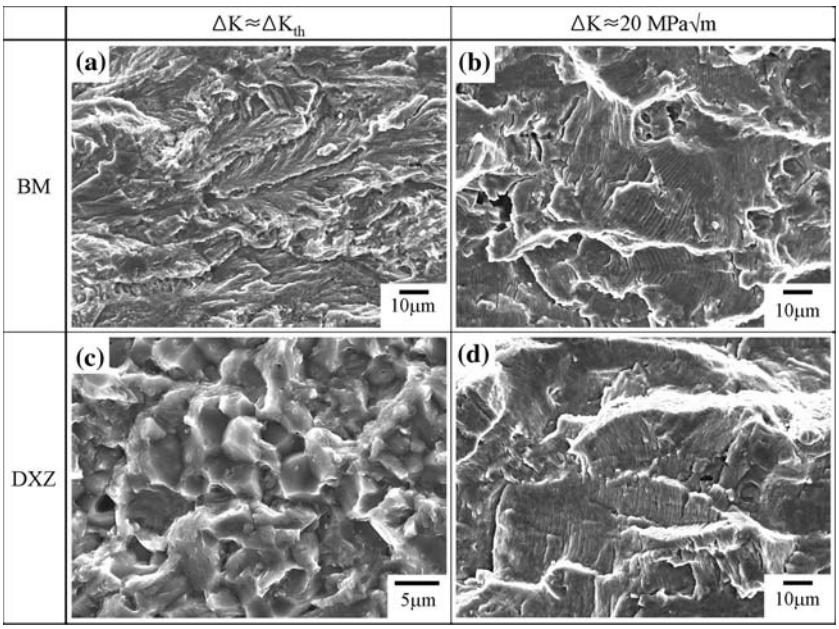

Fig. 5 SEM fractographs of the FSWed 5083-H32 specimens fatigued along the BM at (**a**) $\Delta K \approx 4$ MPa$\sqrt{\text{m}}$ and (**b**) $\Delta K \approx 20$ MPa$\sqrt{\text{m}}$, respectively, and the DXZ at (**c**) $\Delta K \approx 7.5$ MPa$\sqrt{\text{m}}$ and (**d**) $\Delta K \approx 20$ MPa$\sqrt{\text{m}}$, respectively

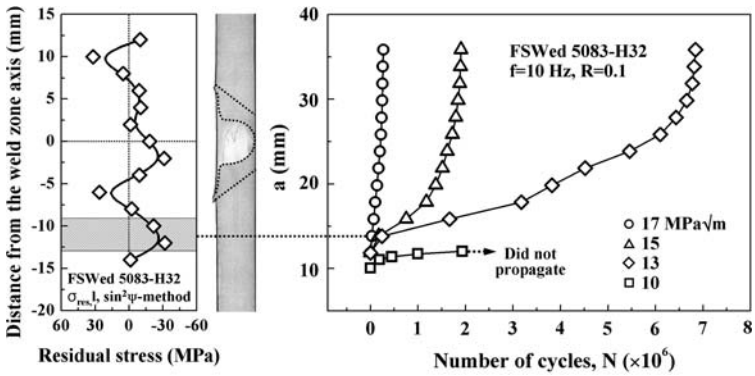

Fig. 6 Fatigue crack length, a, as a function of fatigue loading cycle, N at each applied ΔK for the FCP rates for FSWed 5083-H32 specimen. The FCP tests were conducted perpendicular the weld zone axis at constant ΔK value of 10, 13, 15, and 17 MPa$\sqrt{\text{m}}$, respectively

a–N curve, tends to vary significantly at certain locations, the trend of which depends on the applied ΔK. At an applied ΔK of 17 MPa$\sqrt{\text{m}}$, for example, the FCP rates were not considerably influenced by the presence of FSW zone. At applied ΔK values of 15 MPa$\sqrt{\text{m}}$ and below, the FCP rates became retarded with the crack approaching the weld zone. The fatigue crack retardation at ΔK values of 15 and 13 MPa$\sqrt{\text{m}}$ began at approximately 12 mm away from the weld zone axis, the location of which matches to the RSAZ, as defined in Fig. 3. At both applied ΔK values, the FCP rates recovered from approximately the center of the weld zone due to the residual stress relief with growing crack. At an applied ΔK value of 10 MPa$\sqrt{\text{m}}$, fatigue crack did not even propagate with the crack approaching the RSAZ. The present study suggests that the presence of FSW zone in front of propagating crack retards the FCP rates of 5083-H32 specimen significantly in low and intermediate ΔK regimes due to the longitudinal residual stress acting on the FSW zone.

Conclusions

In this study, the FCP behavior of FSWed 5083-H32 specimen was examined with the fatigue crack growing either along the DXZ at variable ΔK or perpendicular to the DXZ at a constant ΔK value of 10, 13, 15, and 17 MPa$\sqrt{\text{m}}$, respectively, and the following conclusions are drawn.

1. The FCP rates in the DXZ tended to be significantly lower than those in the BM particularly in low and intermediate ΔK regimes. The FCP behavior of FSWed 5083-H32 specimen in the DXZ appeared to be determined by the beneficial compressive residual stress reducing effective ΔK and the detrimental grain refinement causing intergranular fatigue failure.
2. The constant ΔK fatigue test across the weld zone showed that crack retardation occurred far beyond the thermomechanically affected zone (TMAZ) at low ΔK

regime. The present study strongly suggests that the presence of FSW zone in front of propagating crack retards the FCP rates of 5083-H32 specimen significantly in low and intermediate ΔK regimes due to the longitudinal residual stress acting on the FSW zone.

Acknowledgements This research was supported by a grant from the Center for Advanced Materials Processing (CAMP) of the 21st Century Frontier R&D Program funded by the Ministry of Science and Technology, Korea. This research was also supported by the second stage of BK21 project.

References

1. Salem HG, Reynolds AP, Lyons JS (2002) Scripta Mater 46:337
2. Lim SG, Kim SS, Lee CG, Kim SJ (2004) Metall Mater Trans A 35A:2837
3. Lim SG, Kim SS, Lee CG, Kim SJ (2005) Metall Mater Trans A 36A:1977
4. Mahoney MW, Rhodes CG, Flintiff JG, Spurling RA, Bingel WH (1998) Metall Mater Trans A 29A:1955
5. Zhou C, Yang X, Luan G (2002) Scripta Mater 53:1187
6. Lucadamo G, Yang NYC, San Marchi C, Lavernia EJ (2006) Mater Sci Eng A 430:230
7. Park KT, Myung SH, Shin DH, Lee CS (2004) Mater Sci Eng A 371:178
8. Lee JH, Kim HS, Won CW, Cantor B (2002) Mater Sci Eng A 338:182
9. Lim SG, Kim SS, Lee CG, Kim SJ (2005) Met Mater -Int 11:113
10. Hong SJ, Kim SS, Lee CG, Kim SJ (2006) unpublished research
11. Pao PS, Lee E, Feng CR, Jones HN, Moon DW (2003) In: Proceedings of the 4th international symposium on friction stir welding, Park City, May 2003
12. Jata KV, Sankaran KK, Ruschau JJ (2000) Metall Mater Trans A 31A:2181
13. Hong SJ, Kim SS, Lee CG, Kim SJ (2006) Scripta Mater 55:1007
14. Pao PS, Fonda RW, Jones HN, Feng CR, Connolly BJ, Davenport AJ (2005) In: Proceedings of the friction stir welding and processing III as held at the 2005 TMS annual meeting, San Francisco, Feb 2005, 27p
15. Martinez SM, Sathish S, Blodgett MP, Mall S, Namjoshi S (2005) Mater Sci Eng A 399:58
16. John R, Jata KV, Sadananda K (2003) Inter J Fatigue 25:939
17. Bussu G, Irving PE (2003) Inter J Fatigue 25:77
18. Prime MB, Herold TG, Baumann JA, Lederich RJ, Bowden DM, Sebring RJ (2006) Acta Mater 54:4013
19. Buffa G, Hua J, Shivpuri R, Fratini L (2006) Mater Sci Eng A 419:389
20. Rajesh SR, Bang HS, Chang WS, Kim HJ, Bang HS, Oh CI, Chu JS (2007) J Mater Process Tech (in press)